Proceedings of ISFOG 2025
5TH INTERNATIONAL SYMPOSIUM ON
FRONTIERS IN OFFSHORE GEOTECHNICS
Nantes, France | June 9-13 2025

ISBN 978-2-85782-758-0

Exploring Sand Interface Friction Angle: Effects of normal stress, surface roughness, and substrate hardness

A. Seiphoori*, T. N. M. Duong, and Mertcan Geyin

Norwegian Geotechnical Institute (NGI), USA
ali.seiphoori@ngi.no

ABSTRACT: This study investigates the effects of surface roughness, substrate hardness, and normal stress on sand residual interface friction angle δ_{res} using a Bromhead ring shear device. Three sands – a fine silica sand, Hokksund sand, and Ottawa sand –were tested against three interface materials (steel, silicon carbide sandpapers, and polypropylene) subject to normal stresses ranging from 10 to 50 kPa, corresponding to an equivalent depth of approximately 5–8 meters in typical offshore soils. Additionally, the inherent variability of the tested sands allows for an investigation into the effects of gradation and particle shape on δ_{res}. A new parameter, the substrate-to-sand hardness ratio (η_H), was introduced to account for the influence of interface hardness. Results revealed that higher normal stresses increased δ_{res}, likely due to enhanced grain-interface interlocking, though the effect was less pronounced for Hokksund sand and silica sand with irregular particle shapes and higher angularity. For polypropylene, the inherent smoothness of the interface dominates over surface roughness, suggesting roughness alone is insufficient to fully characterize interface properties. An empirical model was developed to predict δ_{res} based on key parameters, including surface roughness, hardness, applied normal stress, sand internal friction angle and median particle size. Our findings provide new insights into the role of interface geometry and material-dependent properties in controlling sand-interface friction, enhancing geotechnical predictive modeling and design.

Keywords: Ring shear test; Surface roughness; Substrate hardness; Interface friction angle; Residual shear strength.

1 INTRODUCTION

The residual interface friction angle (δ_{res}) is a crucial parameter in offshore geotechnical design, including but not limited to the design of monopiles, suction buckets, gravity-based foundations or analysis of the pipe-soil interaction and cable routing (Randolph et al., 2005). δ_{res} is typically estimated using ring shear test (e.g., Lemos & Vaughan, 2009; Ho et al., 2011, Quinteros et al., 2017 and 2023, among others), interface shear box (e.g., Ganesan et al., 2014; Wijewickreme et al., 2014; Boukpeti and White, 2017, West-gate et al., 2021), or tilt table tests (Houhou et al, 2020, and 2022). There are various factors affecting the interface-soil friction angle as reported in the literature: (i) grain size, shape, and mineralogy (e.g., Uesugi and Kishida, 1986; Lemos & Vaughan, 2009; Ho et al., 2011); (ii) interface roughness and hardness (e.g., Lemos & Vaughan, 2009; Ganesan et al., 2014; Han et al., 2018); (iii) shearing rate (e.g., Ganesan et al., 2014; Westgate et al., 2018; Martinez and Stutz, 2019; Martinez and Stutz, 2019), and (iv) normal stress (Quinteros et al., 2017), among others. Yet, there is limited knowledge on the relative effects of the particle morphology, mineralogy, and interface material properties especially how the surface hardness may influence the interface friction angle.

The interface friction angle for sand grains against an interface can vary depending on the mode of interaction, which may involve rolling, sliding, and plowing friction, or a combination of these mechanisms (Figure 1). Particles angularity will result in a higher rolling friction coefficient (μ_R) due to further interlocking and surface asperities compared to smooth and rounded particles. Rougher surfaces typically lead to a higher sliding friction coefficient (μ_S) due to increasing mechanical resistance at the contact points. The relative hardness of the particles and the interface dictates the deformation of the interface, leading to plowing friction interaction (Komvopoulos et al., 1986; Kamminga and Janssen, 2007). In this study, we examined three different sands and a range of interface materials with different hardness to investigate the substrate hardness effects along with the surface roughness and normal stress.

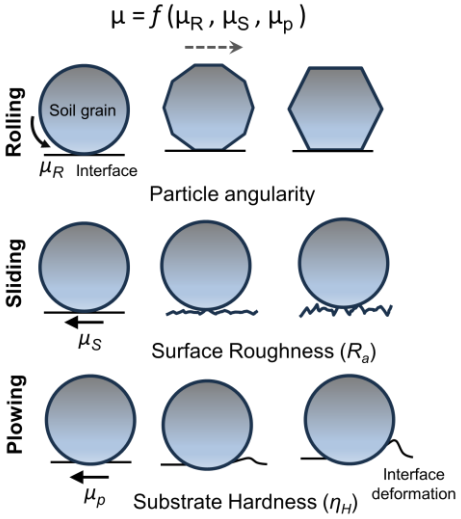

Figure 1. Effects of particle shape, surface roughness, and substrate hardness on the interface friction behavior of sand.

2 MATERIALS AND METHODS

2.1 Sands

Three sand materials including a fine silica sand (Sa), Hokksund sand (HSa), and Ottawa sand (OSa) were used in this research: silica sand with 99.8% content of SiO_2 originated from the lower Greensand formation in Bedfordshire in the United Kingdom, Hokksund a natural glacial-fluvial sand (major components include 35% silica, 25% Na–Feldspar, 20% K–Feldspar, 10% Mica, 5% Amphibole, and 5% other) acquired from Hokksund (Drammen, Norway), and Ottawa sand #20–40, which is entirely silica. Silica sand particles were rounded to subangular, with a nominal grading of more than 99% passing 0.6 mm and less than 1% passing 0.063 mm and Hokksund is a uniform medium-grained sand with 90% of the particles smaller than 1 mm. Ottawa sand (#20–40) features rounded to well-rounded particles, enabling an assessment of the effects of particle morphology through comparing with Hokksund. The index properties and optical images of the above-described materials are presented in Table 1 and Figure 2, respectively.

Table 1. Index and physical properties of the tested sands.

Sand	G_s	D_{50} (mm)	φ'_{cs} (°)	H_s
Silica (Sa)	2.65	0.20	35.2	7.0
Hokksund (HSa)	2.70	0.50	38.2	5.8
Ottawa (OSa)	2.65	0.60	32.8	7.0

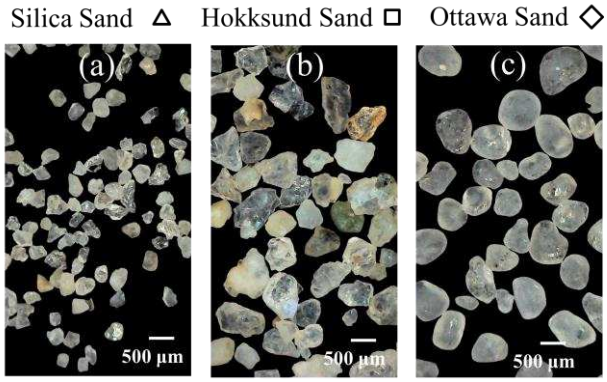

Figure 2. Optical images of the tested sands, including (a) silica sand (Sa); (b) Hokksund sand (HSa); (c) Ottawa sand (OSa), along with their symbols in this study.

2.2 Surface Roughness

A Mitutoyo profilometer (Surftest SJ-310 Series) was used to measure the average surface roughness (R_a), defined as arithmetic mean of the absolute ordinate values y(x) within a sampling length:

$$R_a = \frac{1}{L}\int_0^L |y(x)|dx \qquad (1)$$

where L is the total scanning length (here L= 4 mm), and y(x) is the elevation of the profile at point x. Three types of interface materials, including stainless steel, silicon carbide sandpapers, and polypropylene were tested in this study with R_a varying for two orders of magnitude: smooth stainless steel (R_a = 0.13 μm), sandpaper SP1000 (Grid No. 1000, R_a = 3.61 μm), sandpaper SP220 (Grid No. 220, R_a = 13.27 μm), and polypropylene PPL (R_a = 2.75 μm). Typical roughness profiles for each interface material, along with their optical images, are shown in Figure 3.

2.3 Substrate hardness

The hardness of each interface substrate material (H_i) was evaluated using the Mohs scale. The steel plate's hardness ranged from H = 4–5, matching the hardness of steel pile surfaces (H = 4–8). Similarly, the hardness of polypropylene and sandpaper was evaluated to be in the range of 1–2 and 9–10, respectively. Thus, the steel plate was the smoothest, while the polypropylene plate was the softest. The hardness of the silica sand and Ottawa sand was assumed to be 7.0, while the hardness of Hokksund sand was estimated to be 5.8, calculated as a weighted average of its constituent minerals. We define a new parameter, substrate-to-sand hardness ratio, $\eta_H = \frac{H_i}{H_s}$, to characterize the effects of plowing through the softer material asperities. For instance, η_H for Ottawa sand against polypropylene and sandpaper is 0.21 and 1.36, respectively.

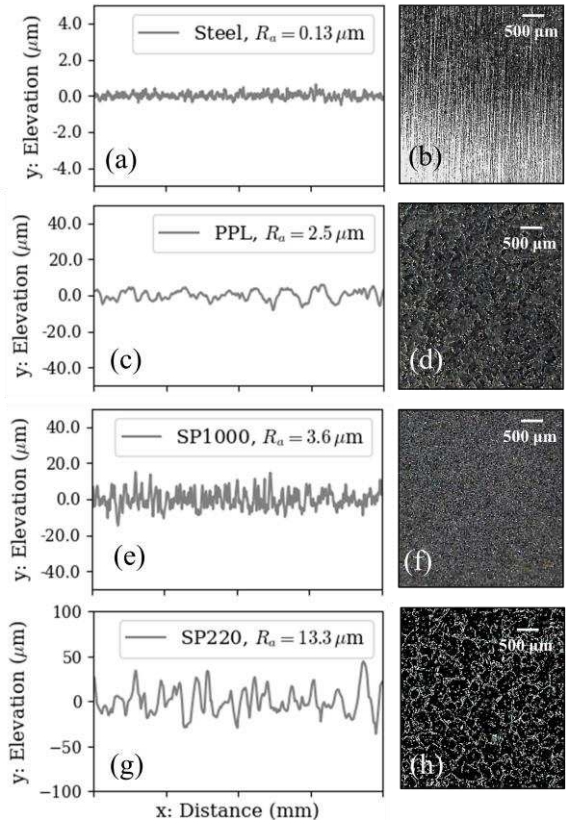

Figure 3. Typical roughness profiles and optical images of the interface plates, including: (a, b) smooth stainless steel; (c, d) polypropylene; (e, f) medium rough sandpaper; and (g, h) rough sandpaper.

2.4 Ring shear device

The schematic diagram of the Bromhead-type (Bromhead, 1979) ring shear device (TORSHEAR, CONTROLS group) modified for interface testing and used in this study is presented in Figure 4. An annular specimen is placed between the outer and inner rings, and the specimen is sheared from its bottom surface. A fixed platen on the top surface measures the soil specimen's resistance to shearing (torque, T) through two torque arms. The specimen's area and depth are 40 cm^2 and 5 mm, respectively. The horizontal loads (F_1 and F_2) are measured using two 1kN loadcells. The normal load is denoted by F_N with the normal loadcell's capacity of 5kN. The normal and shear stress are calculated using the following equations (see ASTM 6467):

$$\sigma_n' = \frac{4F_N}{\pi(D_2^2 - D_1^2)} \qquad (2)$$

$$\tau = \frac{6(F_1+F_2)L}{\pi(D_2^3 - D_1^3)} \qquad (3)$$

where, D_1 and D_2 are the inner and outer specimen diameters and L is the torque arm length (Figure 4a and b).

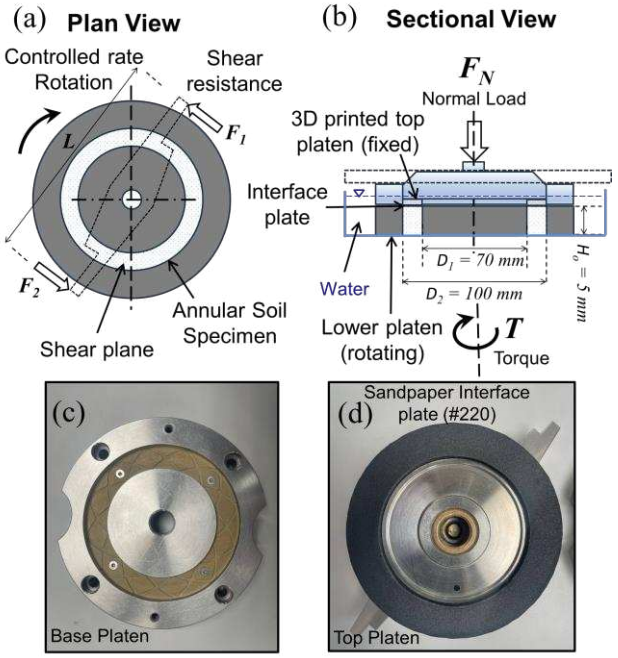

Figure 4. Schematic diagram of the interface ring shear device used in this study: (a) plan view of the lower rotating platen; (b) sectional view of the cell; and (c) base platen, (d) top platen with mounted sandpaper interface plate (SP220).

The interface friction angle is computed as $\delta = tan^{-1}\left(\frac{\tau}{\sigma_n'}\right)$. In this study, the top platen of the Bromhead ring shear device was modified to accommodate different interface plates for soil-interface testing. The interface sheets were epoxied to the top cap of the ring shear device (See Figure 4c and d). The specimens were prepared by pouring materials under dry conditions from a minimum height, resulting in average bulk densities of 1.53, 1.47, and 1.57 g/cm^3 for silica sand, Hokksund sand, and Ottawa sand, respectively. Samples were inundated, and subjected to target normal stresses for 20 minutes, and were then sheared at the rate of 6 mm/min and to a maximum shear rotational displacement of 200 mm. The residual interface friction angle was averaged for the shear displacements > 70 mm. No tests exhibited excessive displacements throughout consolidation and shear phases, complying with previous studies indicating that side friction in the Bromhead apparatus may be considerable for vertical displacements beyond 0.75 mm (Stark and Vettel, 1992).

3 RESULTS AND DISCUSSION

3.1 Critical State Friction Angle

We determined the critical state internal friction angle (φ_{cs}') of the tested materials (Sa, HSa, and OSa) using direct simple shear test (GDS, EMDCSS) under a constant load drained condition (normal effective stress, σ_{vc}' = 25 kPa). Simple shear specimens (height = 20 mm; diameter = 63.5 mm) were subjected to drained shear at a rate of 5%/hour (ASTM D6528). φ_{cs}' values are summarized in Table 1.

3.2 Effect of normal stress

Figure 5 shows the variation of shear stress and interface friction angle versus rotational displacement for Ottawa sand (OSa) sheared against the sandpaper interface SP1000 under different applied normal stresses. The test ID specifies the test type, sand type, normal stress, and interface material. As the normal stress increased, the peak interface friction angle (δ_{peak}) became more pronounced, highlighting the influence of normal forces on the sand-interface interlocking behavior.

Figure 6 shows the variation of δ_{res} with normal stress for all tested sands (Sa, OSa, and HSa) and interface materials (Steel, PPL, SP1000, and SP220). A slight increase in the interface friction angle with the applied normal stress was observed, especially for more rounded OSa particles. Further densification (without particle crushing) of sand particles at higher normal loads may also contribute to the higher interface friction angle. This behavior, however, is less pronounced for HSa and Sa sands. Although HSa and OSa have comparable D_{50}, the irregularity of HSa sand particles may have resulted in a higher contact area, leading to a larger residual friction angle. It is noted that despite the significant difference in surface roughness between the steel and polypropylene interface plates, they produced comparable δ_{res} values (Figure 6a and b).

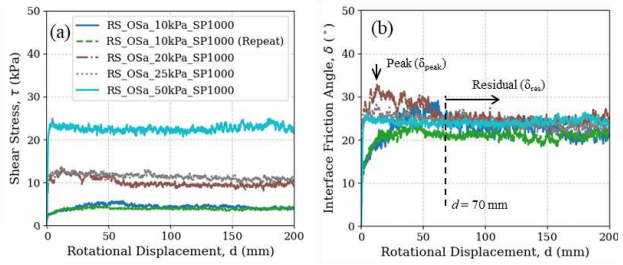

Figure 5. Variation of the shear stress (τ) and interface friction angle (δ) for Ottawa sand sheared against the sandpaper interface plate SP1000 with R_a= 3.6 μm and η_H=1.36.

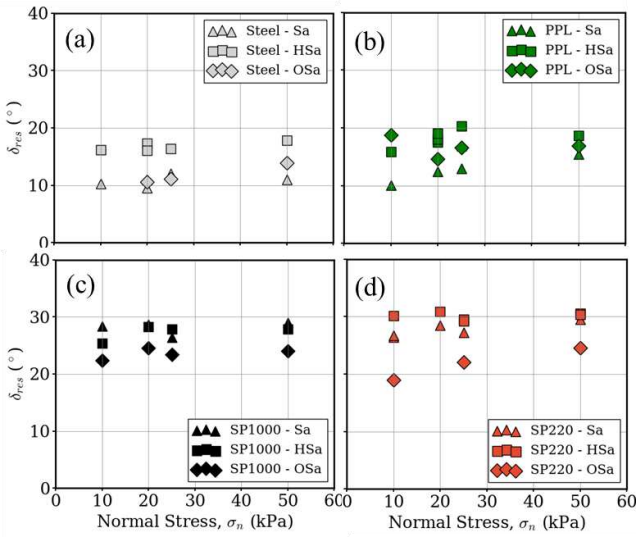

Figure 6. Effect of normal stress on the residual interface friction angle of the tested sands against: (a) Steel; (b) polypropylene; (c) Sandpaper (SP1000); and (d) Sandpaper (SP220).

On the other hand, sandpaper SP1000 with comparable surface roughness to polypropylene interface resulted in much higher δ_{res} values (Figure 6c). This observation suggests that the inherent smoothness of polypropylene plays a more dominant role than its roughness geometry in controlling sand interface friction behavior. It is also observed that the response of OSa sand to an increase in surface roughness from SP1000 to SP220 differs from that of HSa and Sa sands. This difference may be attributed to the greater roundness of OSa sand particles and their dominant frictional mode (see Figures 1 and 2).

3.3 Effect of surface roughness

Figure 7 summarizes the normalized residual interface friction angle versus normalized surface roughness for the tested materials and interface plates, except the polypropylene. In general, the interface friction angle increases at a decreasing rate as the interface roughness increases. A distinct behavior is observed where δ_{norm} increases with normalized roughness, R_{norm}, independent of particle size and shape, likely to be asymptote at δ_{norm} of 1. In the same plot, the effect of normal stress magnitude on δ_{norm} is evident. It is noted that the internal friction angle of the tested sand may depend on the normal stress, demanding further investigation. Additionally, the results for the PPL interface plate were not included in Figure 7. As previously noted, δ_{res} does not follow the surface roughness effect for PPL, highlighting the importance of the substrate material's deformation properties.

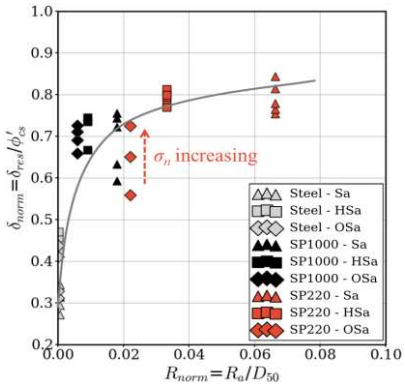

Figure 7. Effect of surface roughness on the residual interface friction angle of the tested sands.

3.4 Effect of substrate hardness

Figure 8 presents the effect of substrate hardness on the residual interface friction angle. Results are plotted in terms of δ_{norm} and the previously defined substrate-to-sand hardness ratio, η_H. A lower η_H for PPL indicates greater deformation of the interface by the sand grains during shearing, suggesting the presence of a plowing-type interaction mechanism. Although PPL has much greater surface roughness, the deformation of the substrate is likely the primary factor contributing to the higher interface friction angle compared to the steel interface. When $\eta_H = 1$, the sand and interface have equal hardness, and no substrate deformation is expected.

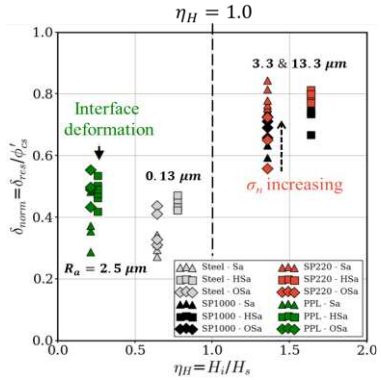

Figure 8. Effect of substrate hardness on the residual interface friction angle of the tested sands.

4 MODELING INTERFACE FRICTION BEHAVIOR

We propose an empirical relationship to predict the residual interface friction angle considering η_H, R_{norm}, σ_n and φ_{cs}'. Even though inherently empirical in nature, the model has a functional form that reasonably captures the combined effects of the input parameters:

$$\frac{\delta_{res}}{\varphi_{cs}'} = 0.40\left(\eta_H + R_{norm}\left(4.84 + 7.58\frac{\sigma_n}{p_a}\right) + \frac{\frac{\varphi_{cs}'}{180^o}}{R_{norm}+\eta_H}\right) \quad (4)$$

where, p_a is atmospheric pressure in the same units of σ_n. Modeling was conducted using simulated annealing, testing billions of functional form combinations and assigning each a complexity score. The loss function used was the Root Mean Square Error (RMSE). A 20/80 train/test split ratio was applied for cross-validation to enhance the model's generalizability. Figure 9a compares model predictions with observations across different materials, while Figure 9b illustrates the errors across various prediction ranges. The errors appear generally homoscedastic, with a slight overestimation observed (0.66 ± 2.19).

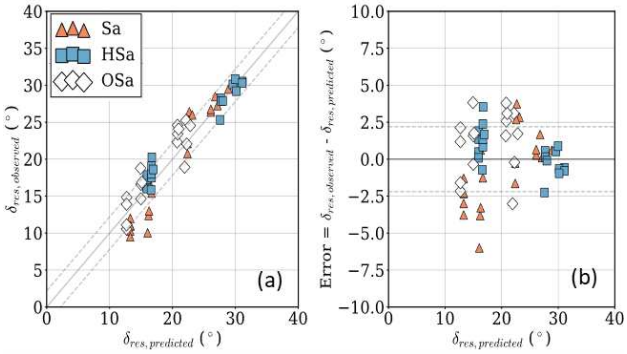

Figure 9. (a) Predicted versus actual residual friction angle; (b) errors in predictions.

5 CONCLUSIONS

Here we studied the interface shear behavior of a range of sand materials using a modified ring shear device, exploring the effects of normal stress, surface roughness, and substrate hardness on δ_{res}.

Key findings are as follows:

Interface friction and *normal stress effects*: As the normal stress increased the peak interface friction angle generally became more pronounced, highlighting the influence of normal forces on the grain-interface interlocking behavior.

Surface roughness and substrate hardness: A critical normalized surface roughness, beyond which δ_{res} plateaus, meaning that further increase in surface roughness does not significantly affect the interface friction angle. Despite the significant difference in surface roughness between the steel and polypropylene interface plates (0.13 µm and 2.5 µm, respectively), they produced comparable δ_{res} values. This suggests that the inherent smoothness of polypropylene plays a more critical role than its roughness in influencing interface friction behavior. A

lower η_H for softer materials such as polypropylene indicates greater deformation of the interface by the sand grains during shearing that in return may increase friction angle.

Modelling sand interface friction: Interface friction angle is a complex parameter, demanding a robust modeling approach. We propose an empirical relationship to predict the residual interface friction angle, considering η_H, R_{norm}, σ_n and φ_{cs}' (six total parameters), that accounts for both stress state and material properties, including the applied normal stress, sand gradation and internal friction angle, and interface roughness and hardness. The model was developed by optimizing numerous functional forms, and A 20/80 train/test split ratio was applied for cross-validation to enhance the model's generalizability. The proposed relationship provides a valuable tool for predicting interface friction angles, though further data are needed to refine and enhance the model to include also particle shape characteristics such as sphericity and roundness.

AUTHOR CONTRIBUTION STATEMENT

A. Seiphoori designed the research and wrote the manuscript. **T. Duong** and **A. Seiphoori** performed experiments and analyzed data**. M. Geyin** developed the empirical model and contributed to analyzing data.

ACKNOWLEDGEMENTS

The authors declare that this research received no specific grant from any funding agency, commercial, or not-for-profit sectors. Support of NGI, Inc., Houston is greatly appreciated.

REFERENCES

Boukpeti, N., & White, D. J. (2017). Interface shear box tests for assessing axial pipe–soil resistance. *Géotechnique*, 67(1), pp.18–30.

Bromhead, E. N. (1979). A simple ring shear apparatus. Ground engineering, 12(5).

Ganesan, S., Kuo, M., & Bolton, M. (2014). Influences on pipeline interface friction measured in direct shear tests. *Geotechnical Testing Journal*, 37(1), paper GTJ20130008.

Ho, T. Y. K., Jardine, R. J., & Anh-Minh, N. (2011). Large-displacement interface shear between steel and granular media. *Géotechnique*, 61(3), pp. 221–234. https://doi.org/10.1680/geot.8.P.086.

Houhou, R., Mjahed, R. B., Sadek, S., & Najjar, S. (2020, February). Drained interface strength between pipelines and clays using tilt table and direct shear tests. *Geo-Congress 2020*, pp. 11–20. Reston, VA: American Society of Civil Engineers.

Houhou, R., Bou Mjahed, R., Sadek, S., & Najjar, S. (2022). Drained Axial Pipe-Soil Resistance at Low Confinement Using Tilt Table and Direct Shear Tests. *Journal of Geotechnical and Geoenvironmental Engineering*, 148(11), 04022086.

Kamminga, J. D., & Janssen, G. C. A. M. (2007). Experimental discrimination of plowing friction and shear friction. *Tribology Letters*, 25, pp. 149–152.

Komvopoulos, K. N. N. P., Saka, N., & Suh, N. P. (1986). Plowing friction in dry and lubricated metal sliding. *Journal of Tribology*, 108(3), pp. 301–312.

Lemos, L. J. L., & Vaughan, P. R. (2009). Clay–interface shear resistance. In Selected papers on geotechnical engineering by PR Vaughan, pp. 392–401. Thomas Telford Publishing.

Ludema, K. C., & Tabor, D. (1966). The friction and visco-elastic properties of polymeric solids. *Wear*, 9(5), pp. 329–348.

Quinteros, V. S., Dyvik, R., & Mortensen, N. (2017). Interface friction angle soil-on-steel from ring shear tests on offshore north sea sands. In *Geotechnical Frontiers 2017*, pp. 358–367.

Quinteros, V. S., Westgate, Z., Vinck, K., Dantal, V., Lindtorp, A., & Toma, M. A. (2023). Interface friction angle of glauconitic sands for pile design. *9th International SUT OSIG Conference "Innovative Geotechnologies for Energy Transition"*, London, UK.

Randolph, M., Cassidy, M., Gourvenec, S., & Erbrich, C. (2005). Challenges of offshore geotechnical engineering. *Proceedings of the 16th international conference on soil mechanics and geotechnical engineering*, pp. 123–176. IOS Press.

Shooter, K. V., & Tabor, D. (1952). The frictional properties of plastics. *Proceedings of the Physical Society*. Section B, 65(9), 661.

Stark, T. D., & Vettel, J. J. (1992). Bromhead ring shear test procedure. *Geotechnical Testing Journal*, 15(1), pp. 24–32.

Westgate, Z., Argiolas, R., Wallerand, R., & Ballard, J. C. (2021, August). Experience with Interface Shear Box Testing for Pipe-Soil Interaction Assessment on Sand. *Offshore Technology Conference* (p. D011S012R004). OTC.

Wijewickreme, D., Amarasinghe, R., & Eid, H. (2014). Macro-scale direct shear test device for assessing soil-solid interface friction under low effective normal stresses. *Geotechnical Testing Journal*, 37(1), paper GTJ20120217.